

# Brownian Dynamics Simulations of a DNA Molecule Colliding with a Small Cylindrical Post

Ju Min Kim and Patrick S. Doyle\*

Department of Chemical Engineering, Massachusetts Institute of Technology, Cambridge, Massachusetts 02139

Received May 9, 2007; Revised Manuscript Received August 9, 2007

**ABSTRACT:** We investigate DNA collisions with a small cylindrical obstacle using BD (Brownian dynamics) simulation and derive the mean hold-up time of hooked DNA molecules based on existing micromechanical models and observations of the present work. Recently, Randall and Doyle (*Macromolecules* 2006, 39, 7734) experimentally explored this DNA collision problem using single molecule microscopy and proposed a set of micromechanical models. They found that so-called X collisions, with increasing total extension during unhooking, are a dominant collision type. Our numerical simulations corroborate that the proportion of X collisions is much higher than that of other collision types for a wide range of Peclet numbers and molecular weights. We compare the predictions of the previously proposed micromechanical models to our simulation results. The derived expressions for the mean hold-up time are consistent with our simulation data and available experimental data for a wide range of Peclet numbers. It is expected that the derived mean hold-up time will be helpful in the design of separation devices using post arrays.

## Introduction

Size-dependent separation of DNA is a key step for DNA mapping and sequencing.<sup>1</sup> Microfabricated or self-assembled post arrays have been considered for the separation of large double stranded DNA.<sup>2–7</sup> Posts have also found application as a means to “preconfigure” DNA before sending it into a microcontraction geometry for stretching.<sup>8</sup> Size separation generally occurs in post arrays because larger DNA have a higher hooking probability and holding time compared to smaller DNA. The hooking and unhooking dynamics around an obstacle has been extensively surveyed.<sup>9–15</sup> The effect of arrangement of post arrays on the separation performance has also been a recent focus for the practical implementation of post arrays.<sup>5–7,14</sup>

In most previous modeling of DNA unhooking dynamics around an obstacle, it was *a priori* envisaged that the DNA molecule is highly stretched in large electric fields and the unhooking step is the most time-consuming portion of the collision process. This fully extended molecule picture results in the rope-over-pulley model,<sup>9,16</sup> which predicts that the average unhooking time scales as  $\sim(E^{-1})^{7,10,12}$  and  $\sim L^{10,12,14}$  in the high electric field limit, where  $L$  is the contour length of the DNA molecule and  $E$  is the electric field. André et al.<sup>11</sup> adopted a trumpet picture<sup>17,18</sup> at intermediate field strengths and a fully extended configuration at high electric field. Their proposed scaling laws for unhooking time were  $E^{-1/3}L^{5/3}$  and  $EL^3$  for freely draining and nondraining cases respectively at intermediate fields. At high electric fields, they predicted that unhooking time scales as  $E^{-1}L^1$  irrespective of hydrodynamic interaction. Dorfman<sup>19</sup> proposed an unhooking time model considering incomplete extension, and argued that a DNA molecule has different conformations depending upon the offset between two arms: taut-chain, stem-flower, and trumpet conformations. He assumed that a DNA molecule always has a stem-flower conformation<sup>18</sup> during unhooking in moderate electric fields. The finite size of a flower portion was considered in his model and the conventional rope-over-pulley model is recovered at

high electric field.<sup>19</sup> Underlying these scaling laws, the probability distribution of arm length is usually assumed to be uniform, e.g., Minc et al.<sup>7</sup> Until recently, it was difficult to directly verify many of the fundamental assumptions due to the lack of systematic analysis of DNA collisions with a single obstacle.

Recently, Randall and Doyle<sup>20</sup> performed single molecule microscopy experiments in which they electrophoretically drove DNA to collide with a small cylindrical post. They classified collision types (W, U/J, and X collisions) into several categories according to the multiplicity of loops and DNA extension at the moment when a short arm starts to retract (the onset of unhooking). One of their most important findings was that the traditional rope-over-pulley model (U/J collisions) was not the most probable collision type. Instead, the collision in which a molecule is simultaneously “extending” during the unhooking (so-called X collision) is dominant. In addition to experimental observations, they proposed micromechanical models to predict the dynamics of U/J and X collisions.

In the previous experimental study of Randall and Doyle,<sup>20</sup> they could only test their models over a limited parameter space and some detailed predictions of the models could not be accurately measured due to experimental limitations. Furthermore, these models were not fully predictive since they required input of the mean stretched chain length as a function of field strength—this parameter will be defined later in the text and denoted by  $\mathcal{L}$ . In addition, application of these models to the problem of DNA separation requires knowledge of the probability distribution of chain conformations at the onset of hooking in order to calculate the *mean* hold-up time for a population of molecules. Previous studies did not examine this aspect of the problem. The primary purpose of this article is to use Brownian dynamics simulations to more fully probe the validity of the previously proposed collision models, derive an expression for  $\mathcal{L}$  that makes these models now fully predictive, and to study trends in the distribution of hooking conformations in order to derive predictions for the mean hold-up time. We will also show that the existence of an X collision does not

\* Corresponding author. E-mail: pdoyle@mit.edu.

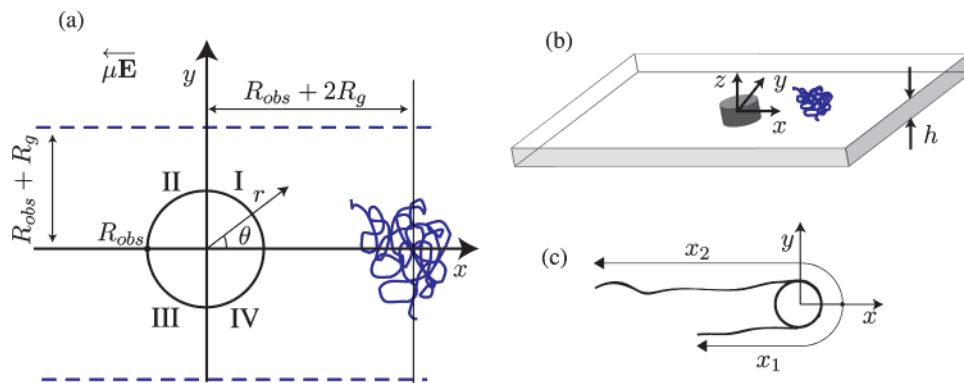


**Figure 1.** (a) Schematic diagram for DNA collision with a single obstacle in a microfluidic channel.  $R_g$  is the radius of gyration of DNA and the cylinder radius ( $R_{\text{obs}}$ ) is  $0.8 \mu\text{m}$ . (b) Side-view of the channel with a cylindrical obstacle, where the channel height ( $h$ ) is  $2 \mu\text{m}$ . (c) Definition of the short arm ( $x_1$ ) and the long arm ( $x_2$ ).  $x_0$  is defined as the difference between  $x_2$  and  $x_1$ . Extension ( $x_{\text{ex}}$ ) is the sum of  $x_1$  and  $x_2$ .

depend on subtle details of the simulation model, but instead it is a general phenomena that was most probably overlooked in previous studies.

### Description of Problem and Method

**Geometry and Observables.** In Figure 1, we present a schematic diagram and definitions for the present study. Geometry and parameters are chosen to coincide with the previous experimental work.<sup>20</sup> We consider single DNA collisions with a single cylindrical obstacle with the radius ( $R_{\text{obs}}$ ) of  $0.8 \mu\text{m}$  in a microfluidic channel with constant height ( $h$ ) of  $2 \mu\text{m}$  and infinite  $x$ - $y$  plane. DNA molecules move in the negative  $x$ -direction by electrophoresis. The field kinematics for the electrophoretic velocity field ( $\mu\mathbf{E}$ ) around a single cylindrical obstacle was previously described in detail by Randall and Doyle.<sup>21,22</sup>

The main observables in this work are the extension of the short arm ( $x_1$ ) and long arm ( $x_2$ ) for hooked DNA, which are measured as the sum of the distance of the left-most part of DNA from  $x = 0$  plus the arc length of one circle quadrant ( $\pi R_{\text{obs}}/2$ ) as shown in Figure 1c. A “hooked” state is the case in which part of the DNA exists in all four quadrants and the DNA chain crosses the  $y$ -axis once at  $y \geq R_{\text{obs}}$  and once at  $y \leq -R_{\text{obs}}$  at any moment, which means that the right semicircle of the cylinder ( $0 < \theta < \pi/2$  and  $3\pi/2 < \theta < 2\pi$ ) is wrapped with a DNA chain (cf. Figure 1c). The extension ( $x_{\text{ex}}$ ) is defined as the sum of  $x_1$  and  $x_2$  and the difference between two arms is defined as  $x_0 = x_2 - x_1$ . Saville and Sevik<sup>12</sup> found that some DNA molecules simply roll over a finite size obstacle without hooking. They called this phenomenon “roll-off”. They also showed that the hold-up time associated with a DNA hooking event is typically an order of magnitude longer than that of a “roll-off” collision. Thus, as done in the previous experimental work,<sup>20</sup> we will focus only on the hooked molecules, which are important in a size-dependent separation device.

We trace DNA molecules starting at  $x_{\text{cm}} = R_{\text{obs}} + 2R_g$  with a random initial  $y_{\text{cm}}$  distribution along  $|y_{\text{cm}}| < R_{\text{obs}} + R_g$  as shown in Figure 1a, and the computations stop when  $x_{\text{cm}}$  reaches  $-L$ . As shown in Figure 2, the collision around an obstacle results in the retarded motion of DNA compared to free electrophoresis. The precollision and postcollision center of mass trajectories are fit to lines with slopes  $\mu E_0$  (Figure 2). The first line starts at  $x_{\text{cm}} = R_{\text{obs}} + 2R_g$  and the second line is fit for  $x_{\text{cm}} < -L/2$ . We determine the hold-up time ( $T_H$ ) as the offset between the two lines.

**Brownian Dynamics Simulation and Parameters.** We model DNA using  $N_b$  beads connected by  $N_s = (N_b - 1)$  springs.

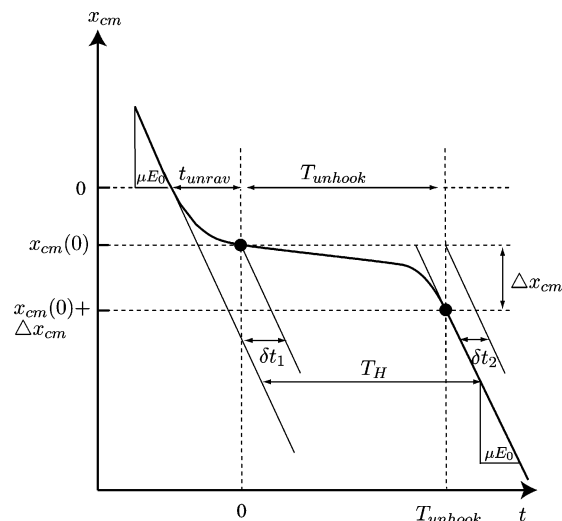


**Figure 2.** Schematic diagram for center-of-mass trajectory of a hooked DNA around an obstacle. The same definitions as the previous experimental work<sup>20</sup> for  $\delta t_1$ ,  $\delta t_2$ ,  $T_{\text{unhook}}$ , and  $T_H$  are used in this work. The left-dot corresponds to the onset of unhooking and the right-dot denotes the moment when unhooking ends.

Hydrodynamic interaction (HI) is not considered since HI is screened in thin slits.<sup>23–25</sup> The excluded volume effect is included since DNA experiments are typically performed in good solvent. Bead–wall interactions are modeled with a modified Heyes–Melrose algorithm.<sup>26,27</sup> We assume electroosmotic flow is negligible.

The evolution equation for bead “ $i$ ” is

$$\frac{d\mathbf{r}_i}{dt} = \mu\mathbf{E}(\mathbf{r}_i) + \frac{1}{\zeta} [\mathbf{f}_i^{\text{B}}(t) + \mathbf{f}_i^{\text{S}}(t) + \mathbf{f}_i^{\text{V}}(t) + \mathbf{f}_i^{\text{ev,wall}}(t)] \quad (1)$$

where  $\mu$  is the bead mobility and  $\zeta$  is the bead drag coefficient.  $\mathbf{f}_i^{\text{B}}$  represents the Brownian force with  $\langle \mathbf{f}_i^{\text{B}}(t) \rangle = 0$  and  $\langle \mathbf{f}_i^{\text{B}}(t_1) \mathbf{f}_j^{\text{B}}(t_2) \rangle = 2k_B T \zeta \delta_{ij} \delta t \mathbf{I}$ , where  $k_B$  is Boltzmann’s constant,  $T$  absolute temperature,  $\delta_{ij}$  Kronecker delta,  $\delta t$  time step and  $\mathbf{I}$  represents the identity tensor.  $\mathbf{f}_i^{\text{S}}$  is the net spring force on the bead.  $\mathbf{f}_i^{\text{V}}$  stands for the force due to excluded volume interaction with other beads.  $\mathbf{f}_i^{\text{ev,wall}}$  denotes bead–wall interactions. The analytical electrophoretic velocity field ( $\mu\mathbf{E}$ ) around a single insulating cylindrical obstacle is used.<sup>21,22</sup> The disturbance to the electric field due to the insulating obstacle quickly decays ( $\sim 1/r^2$ ) as  $r$  increases.<sup>21,22</sup> Thus, for a hooked configuration, most beads lie in a uniform electric field since the DNA length scale ( $L$ ) is much larger than the obstacle size ( $R_{\text{obs}}$ ). Therefore, we adopt the Peclet number ( $Pe$ ) as the principal dimensionless

group in this work, which was also used in the previous experimental work.<sup>20</sup>  $Pe$  is defined as  $\mu E_0 l_p / D$ , where  $D$  is the diffusivity of DNA.  $D$  is equal to  $k_B T / (N_b \zeta)$  since the present simulation is based on a freely draining model.

We adopt the Marko–Siggia (MS) spring force law with effective persistence length<sup>28,29</sup> as follows:

$$\mathbf{f}^s(\mathbf{r}_{ji}) = \frac{k_B T}{\lambda_{\text{eff}} l_p} \left( \frac{r_{ji}}{l} - \frac{1}{4} + \frac{1}{4(1 - r_{ji}/l)^2} \right) \frac{\mathbf{r}_j - \mathbf{r}_i}{r_{ji}} \quad (2)$$

where  $\mathbf{f}^s(\mathbf{r}_{ji})$  stands for force exerted on “ $i$ ” bead by the spring between two connected “ $i$ ” and “ $j$ ” beads.  $l_p$  is the persistence length of unstained DNA ( $0.053 \mu\text{m}^{30}$ ).  $\mathbf{r}_{ji}$  denotes  $\mathbf{r}_j - \mathbf{r}_i$  and  $r_{ji} = |\mathbf{r}_{ji}|$ ,  $l$  is the maximum spring length ( $L/N_s$ ), where  $L$  is the contour length of DNA. Underhill and Doyle<sup>29</sup> introduced a systematic way to determine the effective persistence length to reduce error between the true MS force law and a spring with finite number of persistence lengths, where  $\lambda_{\text{eff}}$  is the ratio of the effective persistence length to true persistence length. We adopted the low-force criterion of Underhill and Doyle.<sup>29</sup> In this work, we consider three different size of DNA molecules,  $\lambda$ -,  $2\lambda$ - and  $T4$ -DNA, which have stained contour lengths of 20.5, 41.0, and  $71.4 \mu\text{m}$ , respectively, for the conditions in ref 20. The number of springs ( $N_s$ ) for  $\lambda$ -,  $2\lambda$ - and  $T4$ -DNA is 37, 74, and 127, respectively, and the corresponding  $\lambda_{\text{eff}}$  value is 1.91, 1.91, and 1.89, respectively. Here, we chose the number of springs so that each spring represents a similar number of persistence lengths.

We use a repulsive soft potential developed by Jendreck et al.<sup>31–33</sup> to incorporate excluded volume effects:

$$U^{\text{ev}}(r_{ij}) = \frac{1}{2} v^{\text{ev}} k_B T N_{K,s}^2 \left( \frac{9}{2\pi R_s^2} \right)^{3/2} \exp \left[ \frac{-9r_{ij}^2}{2R_s^2} \right] \quad (3)$$

where  $v^{\text{ev}}$  is an adjustment parameter for the excluded volume effect,  $N_{K,s}$  stands for the number of Kuhn length per each spring and  $R_s$  is the equilibrium end-to-end distance of each spring.  $v^{\text{ev}}$  was adjusted to match the measured radius of gyration of  $\lambda$ -DNA in free solution. When  $v^{\text{ev}}$  is  $0.0004 \mu\text{m}^3$ , the computed radius of gyration for  $\lambda$ -DNA using an ensemble of 200 molecules is  $0.68 \pm 0.01 \mu\text{m}$  in free solution, which is very close to the measured experimental value of  $0.69 \mu\text{m}$ .<sup>23</sup> On the basis of the radius of gyration of  $\lambda$ -DNA, the radius of gyration for larger molecules in good solvent can be extrapolated with the relationship<sup>34</sup> of  $R_g \sim M_w^{0.589}$ , where  $M_w$  is the molecular weight. The simulated radius of  $T4$ -DNA with  $v^{\text{ev}} = 0.0004 \mu\text{m}^3$  is  $1.44 \pm 0.03 \mu\text{m}$  which is near to the extrapolated value of  $1.42 \mu\text{m}$ . We adopt a modified Heyes–Melrose algorithm<sup>26,27</sup> to deal with bead–wall interactions ( $\mathbf{f}_i^{\text{ev,wall}}$ ). In the modified Heyes–Melrose algorithm,<sup>26,27</sup> the location of a bead is moved to the nearest boundary if a given bead is located out of boundary after a time step, where all boundaries (obstacle, upper and bottom walls) can be analytically defined in this work. In this work, we adopt “adaptive time-stepping” scheme<sup>27</sup> to solve eq 1 and set time step to  $1.25 \times 10^{-4} \times (\zeta l^2 / (k_B T))$  at  $Pe = 64$  and the time step scales as  $1/Pe$  for other conditions.

### Classification of Collisions

In Figure 3, we present the snapshots of representative collision types: U, J, X (“extending”) and W collisions for  $T4$ -DNA at  $Pe = 8$ . The same classification was used in the previous experimental work,<sup>20</sup> and they derived micromechanical models corresponding to each collision type. From Figure

3, we can intuitively understand the various collisions. U collisions correspond to DNA molecules with roughly symmetric arms around an obstacle as shown in Figure 3a. During a U collision a molecule typically has a long hold-up time (cf. a time of 220 has elapsed between the fourth and fifth snapshots in Figure 3a). J collisions show an unsymmetrical configuration of the two arms and there is usually no long flat region in the center-of-mass trajectory (see Supporting Information). In Figure 3c, we present a typical X collision, where the coiled part of a long arm is continuously extending up to the end of unhooking. The speed of the coiled region is constant (cf. the time step between two successive snapshots is almost constant). This affine motion of the coil portion of the chain for X collisions was assumed in the model of Randall and Doyle.<sup>20</sup> We finally present a W collision which corresponds to hooking with two loops in Figure 3d. This W collision corresponds to a “metastable” state, which will be explained later.

We classify collisions in a similar way as the previous experimental study.<sup>20</sup> First, we classify the collision types according to the multiplicity of loops around the cylinder: W and non-W collisions (U/J and X collisions). While a DNA molecule is in a “hooked” state around the obstacle, we define a W collision as the case that both ends of DNA are in the same quadrant. Among molecules in the W configuration, those that fluctuate out of a W state any time before unhooking are called “metastable” W molecules. We classify U, J, and X collisions according to the amount of extension ( $x_{\text{ex}}$ ) when a short arm starts to retract. We define U and J collisions as those with extension values close to  $\mathcal{L}$ , denoting molecules with  $x_{\text{ex}}/\mathcal{L} \geq 1 - \delta_{\text{cr}}$  as U and J collisions and those with  $x_{\text{ex}}/\mathcal{L} < 1 - \delta_{\text{cr}}$  as X collisions, where  $\delta_{\text{cr}}$  is a specified criterion that we set to 0.1 as done in the previous experimental work.<sup>20</sup> We checked other  $\delta_{\text{cr}}$  values to analyze the sensitivity of the classification to this criterion (see Supporting Information).

We computed  $\mathcal{L}$  at a given  $Pe$  as follows. We considered a symmetric configuration of the two arms around a cylinder. With the center bead fixed on the cylinder ( $\theta = 0$ ), we obtained  $\mathcal{L}$  as the average steady-state extension  $x_{\text{ex}}$ . For this calculation, we always used an odd number of beads (39, 75, and 129 beads for  $\lambda$ ,  $2\lambda$ , and  $T4$ -DNA, respectively). To determine the effect of bead number, we used both 37 and 39 beads for  $\lambda$ -DNA and found that this did not affect the average  $x_{\text{ex}}$ .

### Models for Hooking and Unhooking Dynamics

In this section, we briefly summarize the models of Randall and Doyle<sup>20</sup> for DNA collisions. The definitions  $\delta t_1$ ,  $\delta t_2$ ,  $T_{\text{unhook}}$  and  $T_{\text{H}}$  presented in Figure 2 are the same as the previous experimental work.<sup>20</sup> In Figure 2, the left-dot corresponds to the onset of unhooking and the right-dot denotes the end of unhooking.  $T_{\text{unhook}}$  corresponds to the interval between the two dots.  $t_{\text{unrav}}$  is the interval between the onset of hooking and the onset of unhooking ( $t = 0$ ), where the onset of hooking corresponds to the moment when  $x_{\text{cm}} = 0$  and the onset of unhooking denotes the moment when a short arm starts to retract.  $\Delta x_{\text{cm}}$  corresponds to the center-of-mass displacement during unhooking. Randall and Doyle<sup>20</sup> defined a characteristic time  $t_c = \mathcal{L} / \mu E_0$  which corresponds to the convective time scale that it takes a DNA to move a distance  $\mathcal{L}$  with free electrophoretic velocity ( $\mu E_0$ ). Last,  $x_1(0)$  is the length of a short arm at the onset of unhooking ( $t = 0$ ). The summary of J and X models are given below.

**J Model.** Randall and Doyle<sup>20</sup> derived the equation for unhooking dynamics based on constant partial extension ( $\mathcal{L}$ ) during unhooking, which is basically equivalent to the conven-

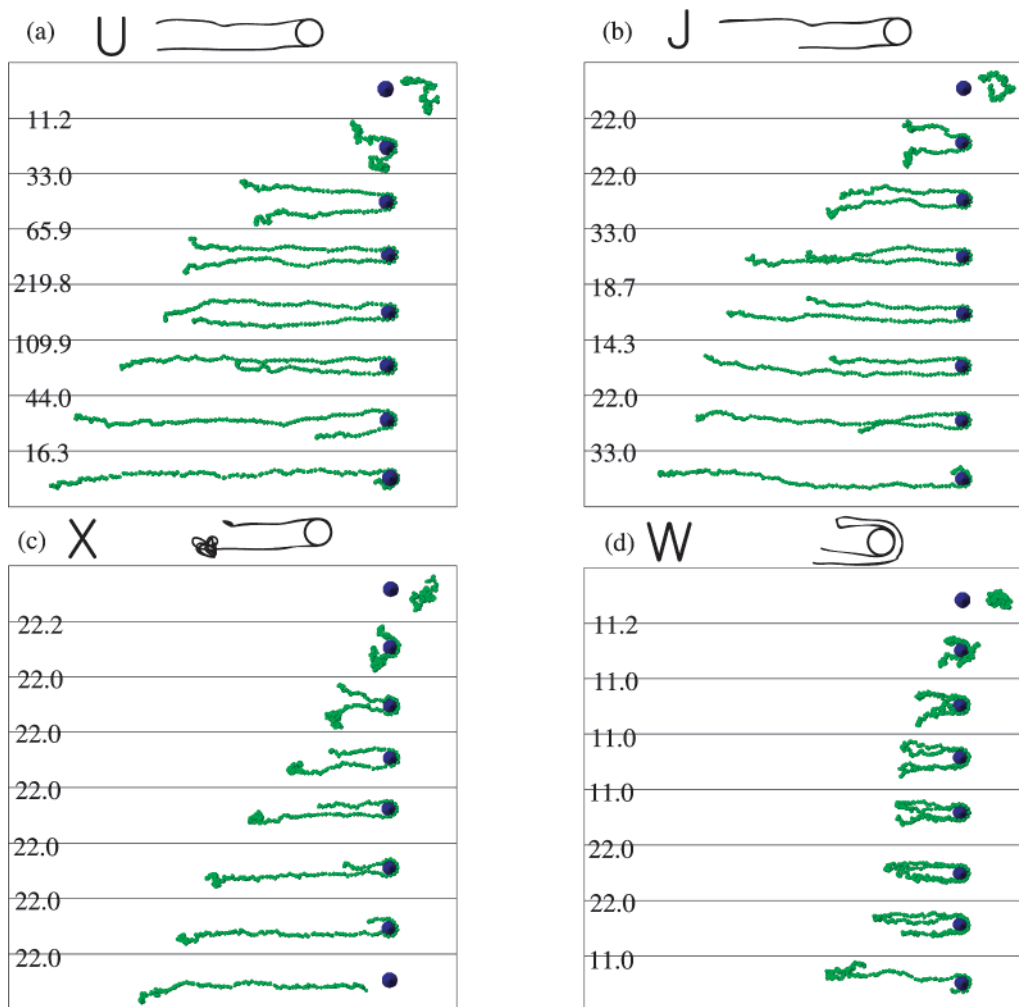


**Figure 3.** Representative examples of (a) U, (b) J, (c) X, (d) W collisions for T4-DNA at  $Pe = 8$ . The numbers on the left side of the images correspond to the dimensionless time ( $\equiv \Delta t/(l_p^2/D)$ ) between two successive snapshots.

tional rope-over-pulley model with  $L$  replaced by  $\mathcal{L}$ . Randall and Doyle<sup>20</sup> recognized that  $T_H$  is not  $t_{\text{unrav}} + T_{\text{unhook}}$  but  $T_{\text{unhook}} + \delta t_1 - \delta t_2$  due to the movement of center-of-mass during unraveling and unhooking as shown in Figure 2. In modeling of  $\delta t_1$  and  $\delta t_2$  for J molecules, the partial extension is assumed to be constant.<sup>20</sup> This gives

$$\delta t_1 = t_c [1/2 - (x_1(0)/\mathcal{L})^2] \quad (4)$$

$$\delta t_2 = t_c [(x_1(0)/\mathcal{L}) - (x_1(0)/\mathcal{L})^2] \quad (5)$$

The unhooking time for the J model is

$$T_{\text{unhook}} = -\frac{t_c}{2} \ln(1 - 2(x_1(0)/\mathcal{L})) \quad (6)$$

Combining eqs 4–6 we get:

$$T_H = t_c [-(1/2) \ln(1 - 2(x_1(0)/\mathcal{L})) + 1/2 - (x_1(0)/\mathcal{L})] \quad (7)$$

**X Model.** For an X collision it was assumed that a molecule is composed of two parts: a freely moving coil at the end of the long arm that is connected to a taut chain. The length of the long arm grows as  $\mu E_0 t$  whereas the portion in tension is governed by a ropelike assumption.<sup>20</sup> To derive  $\delta t_1$  and  $\delta t_2$  for X molecules, the center-of-mass for the coil portion was assumed to be located at the end of the long arm and the

remaining part of DNA molecule is straight. The equations for  $\delta t_1$  and  $\delta t_2$  are

$$\delta t_1 = t_c (x_1(0)/\mathcal{L})^2 \quad (8)$$

$$\delta t_2 = t_c [2.1(x_1(0)/\mathcal{L}) - 3.8(x_1(0)/\mathcal{L})^2] \quad (9)$$

The unhooking time for an X collision is<sup>20</sup>

$$T_{\text{unhook}} = 2.1 t_c (x_1(0)/\mathcal{L}) \quad (10)$$

The hold-up time  $T_H$  for an X collision is

$$T_H = 4.8 t_c (x_1(0)/\mathcal{L})^2 \quad (11)$$

From the above equations, the different scaling laws between  $T_H$  and  $T_{\text{unhook}}$  for U/J collisions and X collisions were predicted to be:

$$T_H \sim T_{\text{unhook}} \quad \text{for U/J collisions} \quad (12)$$

$$T_H \sim T_{\text{unhook}}^2 \quad \text{for X collisions} \quad (13)$$

### Hooking and Unhooking Dynamics

**Quantitative Classification of Collision Types.** In Table 1, we classified DNA collisions into U/J, X, and W types. We also present previous experimental data<sup>20</sup> for comparison. First, we observe good agreement between experimentally measured



**Table 1. Classification of Collision Types around a Cylindrical Obstacle for Three DNA Molecules:  $\lambda$ -DNA,  $2\lambda$ -DNA, and T4-DNA**

DNA, $Pe$	simulation:		experiment <sup>20</sup> (-)	
	% (U/J)/% X/% W(% metastable)	$\delta_{cr}=0.1$	$\mathcal{L}^{exp}$	$\delta_{cr}=0.1$
$\lambda$ , $Pe = 2$	6.1	67/33/0(0)	6.6	83/17/0(0)
$\lambda$ , $Pe = 5$	9.9	41/57/2(1)		
$\lambda$ , $Pe = 8$	12.0	32/64/4(1)	13	43/57/0(0)
$\lambda$ , $Pe = 16$	14.6	26/63/11(3)		
$\lambda$ , $Pe = 32$	16.5	24/64/12(5)		
$\lambda$ , $Pe = 64$	17.9	20/65/15(6)		
$\lambda$ , $Pe = 128$	18.7	20/62/18(5)		
$2\lambda$ , $Pe = 2$	11.8	34/65/1(1)		
$2\lambda$ , $Pe = 5$	19.9	26/66/8(3)		
$2\lambda$ , $Pe = 8$	24.1	22/66/12(3)		
$2\lambda$ , $Pe = 16$	29.1	19/65/16(5)		
$2\lambda$ , $Pe = 32$	32.8	22/58/20(6)		
$2\lambda$ , $Pe = 64$	35.6	17/59/24(8)		
$2\lambda$ , $Pe = 128$	37.3	14/62/24(8)		
T4, $Pe = 2$	20.5	25/72/3(1)		
T4, $Pe = 5$	34.9	19/67/14(5)		
T4, $Pe = 8$	41.7	22/61/17(7)	45	29/60/11(5)
T4, $Pe = 16$	50.4	19/61/20(6)		
T4, $Pe = 32$	56.8	15/60/25(10)		
T4, $Pe = 64$	61.5	17/55/28(9)		
T4, $Pe = 128$	64.8	14/58/28(10)		

<sup>a</sup>  $\delta_{cr}$  is a criterion to classify hooking types into U/J or X collision: U/J collision ( $x_{ex}/\mathcal{L} \geq 1 - \delta_{cr}$ ) and X collision ( $x_{ex}/\mathcal{L} < 1 - \delta_{cr}$ ). The values listed in each column are percentages of each collision type for a given parameter set.  $\mathcal{L}^{sim}$  and  $\mathcal{L}^{exp}$  are given in  $\mu\text{m}$ .

extension ( $\mathcal{L}^{exp}$ ) and computed extension ( $\mathcal{L}^{sim}$ ). In Table 1, we observe that X collisions are dominant for a wide range of parameter space and the proportion of X collisions becomes saturated around 60% with increasing  $Pe$ , irrespective of molecular weight. However, the proportion of X collisions is quite dependent upon molecular weight at low  $Pe$ , i.e., the proportion is much smaller in the case of  $\lambda$ -DNA compared to T4-DNA. Randall and Doyle<sup>21</sup> argued that DNA hooking is closely linked with the local field gradient-induced stretching below a critical  $De$  ( $\sim 40$ ), where  $De$  is defined as  $2\mu E_0/R_{obs} \times \tau$  and  $\tau$  is the longest relaxation time. Local field kinematics also become more important with increasing ratio of  $R_{obs}/R_g$ <sup>21</sup> and  $De$  increases with increasing molecular weight at a given  $Pe$ . In brief, field gradient-induced stretching in hooking becomes more important with decreasing molecular weight due to a geometrical effect ( $R_{obs}/R_g$ ) and smaller  $De$  at low  $Pe$ . We speculate that this field gradient-induced stretching results in more U/J collisions for small DNA molecules at small  $Pe$  since

the coiled portion of a DNA molecule is stretched out while the DNA molecule is in front of an obstacle (the impact stage).

The proportion of W collisions gradually increases with increasing  $Pe$  but it also saturates at high  $Pe$  for larger molecules (i.e., 24% and 28% for  $2\lambda$ -DNA and T4-DNA, respectively). Approximately 25–42% of the molecules among the ensemble of W collisions are metastable for  $Pe \geq 8$  irrespective of molecular weight. The proportion of W collisions in the simulation is somewhat larger than seen experimentally.<sup>20</sup> We attribute this difference to possible uncertainty in the visual categorization of W collisions in the experiment. It can be difficult to visually discern W collisions from X collisions due to the possibility of having multiple chain loops in the coiled portion in X molecules.

Prior to this current study, there have been several simulation studies of a polymer colliding with a single obstacle;<sup>10–12,35</sup> however, an X type collision was never reported. To ensure that the presence of this collision type does not arise from subtle differences in our model from that in previous studies, we progressively simplified the model by turning off excluded volume, using simpler spring force laws (FENE<sup>37</sup>) and applying a uniform electric field (i.e., assuming a conducting obstacle). We find that the X collision continues to be the dominant collision type (see Table S2 in Supporting Information). Thus, these results imply that an X collision can be reproduced in simulations so long as a nonlinear spring force is used. Prior work may have not seen this type of collision because they either assumed the initial state of the hooked chain to be in the U/J conformation<sup>11</sup> or were concentrating on other aspects of the problem (such as roll-offs<sup>12</sup>), or simply treated all hooked collisions as one type.

**The Correlation between Unhooking Dynamics and Short Arm Length.** The unhooking step has been known to be the most time-consuming part of the collision process and thus it is believed that unhooking physics plays a key role in understanding DNA collisions with a single obstacle.<sup>20</sup> Here, we will investigate the feasibility of the conventional rope-over-pulley model. In the rope-over-pulley model, the driving force is assumed to be proportional to the difference between arm lengths ( $x_0$ ).<sup>9,10,16,35</sup> Thus, if the rope-over-pulley model is a relevant unhooking mechanism, the hold-up time of most DNA molecules will be correlated with  $x_0(0)$ . Equation 6 for J molecules can be converted to the following equation with

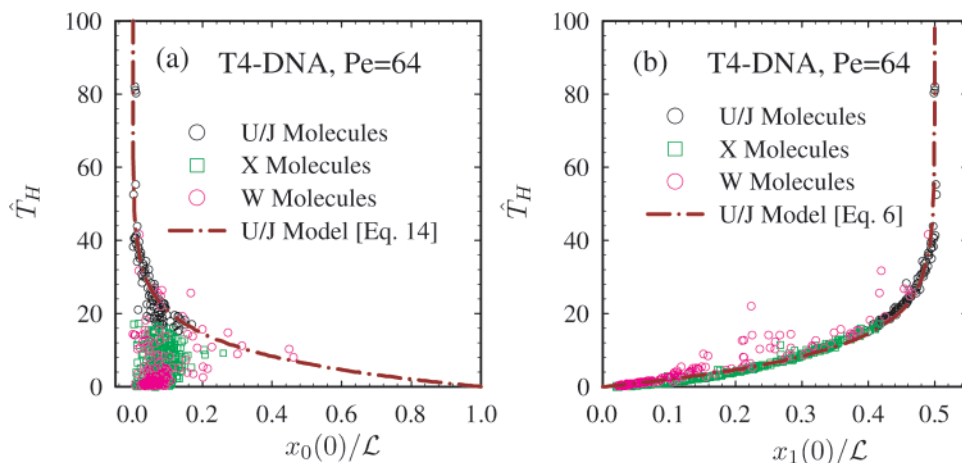


**Figure 4.** Hold-up time distribution for T4-DNA at  $Pe = 64$ , where the hold-up time ( $T_H$ ) is nondimensionalized with  $l_p^2/D$ . (a) Hold-up time distribution for U/J, X, W molecules as a function of the normalized difference between two arm lengths ( $x_0(0)/\mathcal{L}$ ). (b) Hold-up time distribution for U/J, X, and W molecules as a function of normalized short arm length  $x_1(0)/\mathcal{L}$ .

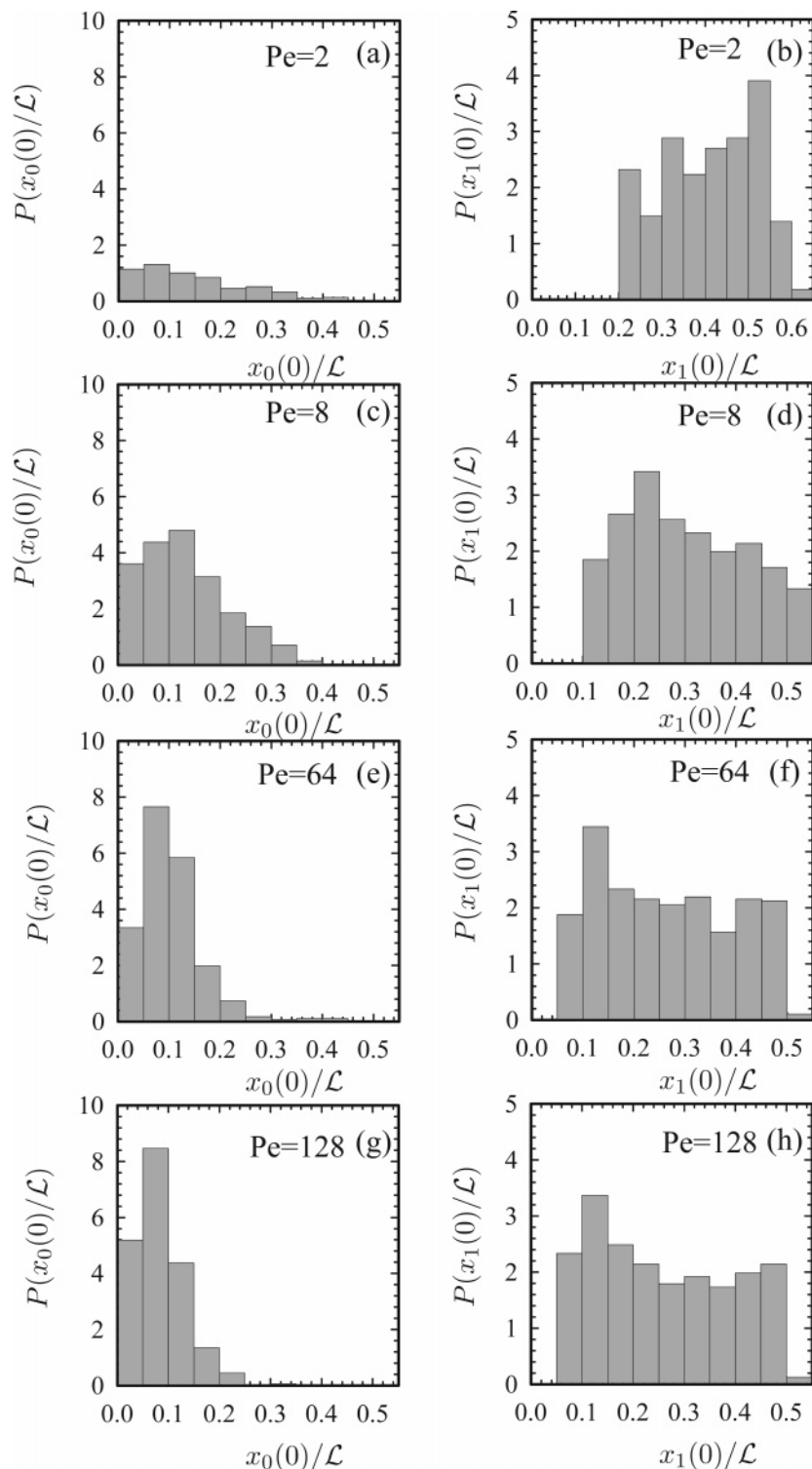


**Figure 5.** Probability distribution of  $x_0(0)/\mathcal{L}$  (left-hand side) and  $x_1(0)/\mathcal{L}$  (right-hand side) at the onset of unhooking for  $\lambda$ -DNA.

variable  $x_0(0)/\mathcal{L}$  ( $\equiv 1 - 2(x_1(0)/\mathcal{L})$ ) as long as the partial extension ( $\mathcal{L}$ ) is constant:

$$T_{\text{unhook}} = -\frac{t_c}{2} \ln(x_0(0)/\mathcal{L}) \quad (14)$$

In Figure 4, hold-up time data are presented for T4-DNA at  $Pe = 64$  vs  $x_0(0)/\mathcal{L}$  (a) or  $x_1(0)/\mathcal{L}$  (b). As shown in Figure 4a, there exists a strong correlation between the simulation results and eq 14 for U/J molecules. However, most X and W molecules (which are the majority of the ensemble (cf. Table 1)) deviate

from eq 14. Thus, we can conclude that the conventional rope-over-pulley model can be applied only to a small portion of the population, at least for the present parameter set. On the other hand, it is observed in Figure 4b that there is a strong correlation between most simulation data and  $x_1(0)/\mathcal{L}$ , except for some of the W molecules. Thus, we can surmise that unhooking dynamics is strongly correlated to short arm dynamics, in accord with the previous experiments<sup>20</sup> and in contrast to all other studies of polymer-post collisions.

**Probability Distribution of Arm Length.** The modeling of mean hold-up time will be helpful in designing a device where

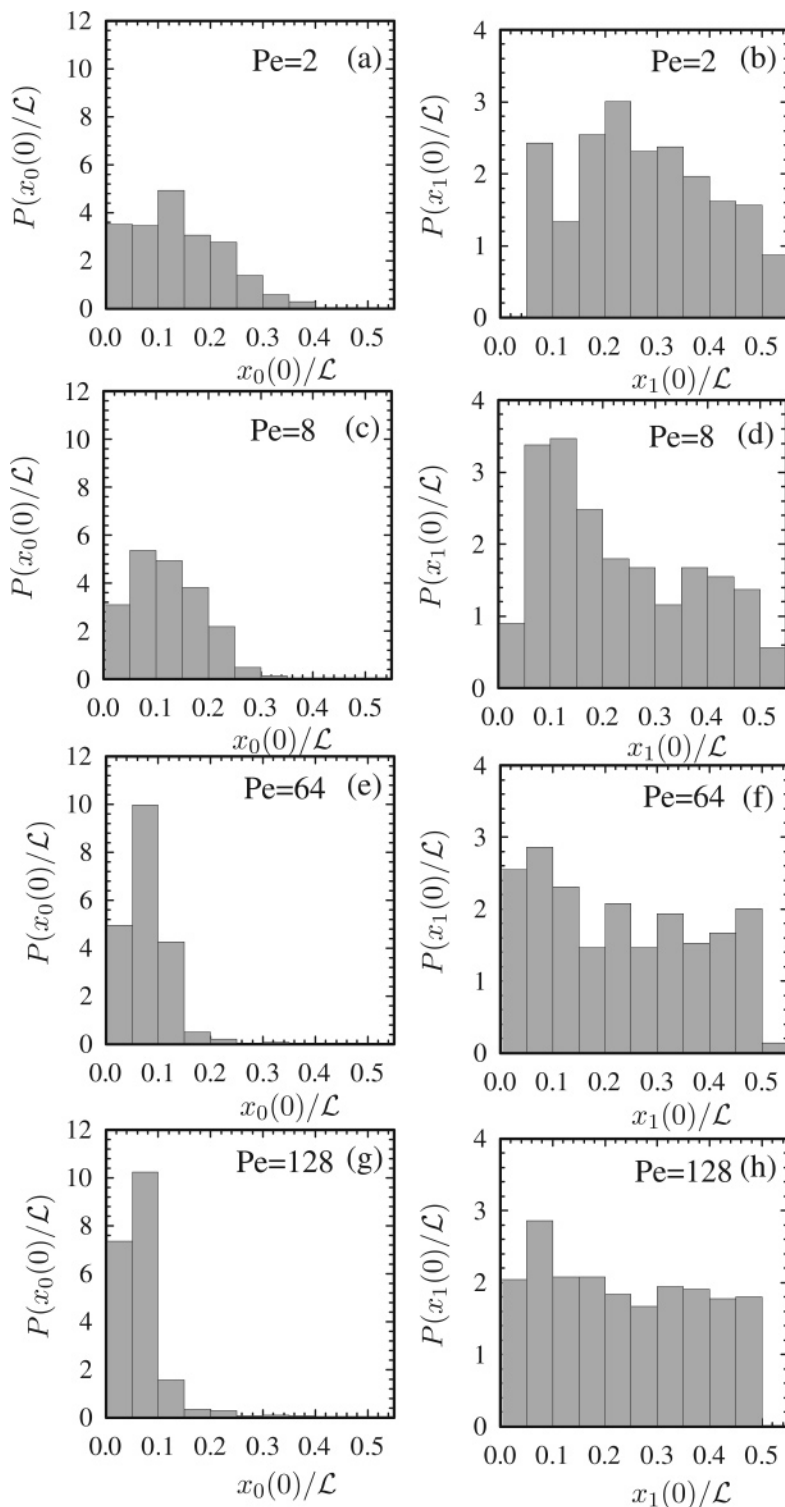


**Figure 6.** Probability distribution of  $x_0(0)/L$  (left-hand side) and  $x_1(0)/L$  (right-hand side) at the onset of unhooking for T4-DNA.

molecular weight dictates the mean hold-up time around an obstacle. The mean hold-time can be computed with the following convolution:

$$\langle T_H \rangle = \int_0^a p(\hat{x}) T_H(\hat{x}) d\hat{x} \quad (15)$$

where  $T_H(\hat{x})$  denotes the micromechanical model for hold-up time and  $p(\hat{x})$  is the probability distribution of  $\hat{x}$ . The model for  $T_H(\hat{x})$  can be the rope-over-pulley model or micromechanical model proposed by Randall and Doyle.<sup>20</sup> In this work, we will look into other heuristic models as well. The dimensionless

variable  $\hat{x}$  can be  $x_0(0)/L$  or  $x_1(0)/L$  depending on the micromechanical model for the hold-up time. The upper limit of the integral,  $a$  is dependent upon  $\hat{x}$ . Up to now, most work has focused on a model for  $T_H(\hat{x})$ . However, from eq 15, it is clear that the probability distribution of  $\hat{x}$  should also be correctly modeled to accurately predict the mean hold-up time. There is no systematic survey of the probability distribution of  $\hat{x}$  in previous experimental or simulation studies. In Figures 5 and 6, we present the probability distributions of  $x_0(0)/L$  and  $x_1(0)/L$  for  $\lambda$ -DNA and T4-DNA. We mention that there is no molecule with  $x_1(0)/L < 0.05$  for  $\lambda$ -DNA since a hook requires

$x_1(0)/L > 0.05$ . In these figures we can observe several trends: the probability distribution of  $x_0(0)/L$  becomes skewed toward smaller values of  $x_0(0)/L$  (Figures 5 and 6: left-hand side) with increasing  $Pe$  while  $x_1(0)/L$  becomes uniform with increasing  $Pe$  (Figures 5 and 6: right-hand side). These trends for  $x_0(0)/L$  and  $x_1(0)/L$  become more pronounced with increasing molecular weight (cf. Figures 5 and 6). Thus, at high  $Pe$ , we can assume the following probability distribution function for  $x_1(0)/L$ :

$$p(x_1(0)/L) = 2 \quad \text{for } 0 \leq x_1(0)/L \leq 0.5 \quad (16)$$

As can be seen from Figures 5a and 6a, the distribution for  $x_0(0)/L$  becomes skewed toward lower values ( $x_0(0)/L \leq 0.1$ ) with increasing  $Pe$  and increasing molecular weight at the onset of unhooking. Thus, we assumed that the probability distribution of  $x_0(0)/L$  at high  $Pe$  is as follows:

$$p(x_0(0)/L) = \begin{cases} 10 & \text{if } x_0(0)/L \leq 0.1 \\ 0 & \text{otherwise} \end{cases} \quad (17)$$

Examining the probability distribution of  $x_0(0)/L$  at high  $Pe$ , we observe that the difference between the two arm lengths is not large at the onset of unhooking for most cases. In Figure 7, we show the relationship between the two arm lengths according to collision types. We can see that the relationship between short and long arm lengths becomes more linear with increasing  $Pe$  for X collisions. In contrast, short and long arm lengths are inversely related for U/J collisions, since the sum of short and long arm lengths is constant. From the relationship between the two arm lengths for X collisions, we note that unhooking in an X collision occurs once the length of the long arm exceeds that of the short arm.

The present observation for an X collision is inconsistent with the conventional rope-over-pulley model in which it was assumed that unhooking starts after a DNA molecule is fully extended. To understand the origin of the unhooking mechanism for X collisions, we consider a DNA molecule in which a single, arbitrary, bead is tethered on an obstacle ( $\theta = 0$ ). The two arms, separated by the tethered bead, start to unravel, mimicking the unraveling step of the DNA collision problem. Recently, Mohan and Doyle analyzed the unraveling phenomenon of a tethered polymer.<sup>36</sup> In the high electric field limit, their analysis shows that the spring force at the tethered point initially increases with the same slope irrespective of molecular weight. However, the spring force becomes saturated at the steady-state value of  $2N_{k,s}Pe^t$ ,<sup>36</sup> where  $Pe^t$  is defined as  $\mu E_0 l_p N_b^t \zeta / k_B T$ . Here  $N_b^t$  is the number of beads in the tethered DNA. Applying this analysis to the current problem, we note that the short arm reaches steady-state more rapidly than the long arm. Thus, as soon as the short arm reaches steady state, the tension of the long arm exceeds that of the short arm, resulting in the onset of unhooking. Therefore, in most cases, at the onset of unhooking, the difference in length between the two arms becomes small irrespective of  $x_1(0)/L$  at high  $Pe$ , as shown in Figure 7. Additionally, the difference corresponds to the size of the coiled portion in a long arm. Finally, we mention that there are some W molecules with a large difference in extension between arms as shown in Figure 7, since some W molecules are changed into J configuration while still hooked (metastable states).

### Comparison of Models with Numerical Data

In Figure 8, we directly compare predictions for  $\delta \hat{t}_1$ ,  $\delta \hat{t}_2$ , unhooking time ( $\hat{T}_{\text{unhook}}$ ) and hold-up time ( $\hat{T}_{\text{H}}$ ) for X (eqs 8–11) and U/J models (eqs 4–7) with simulation data. In this study,

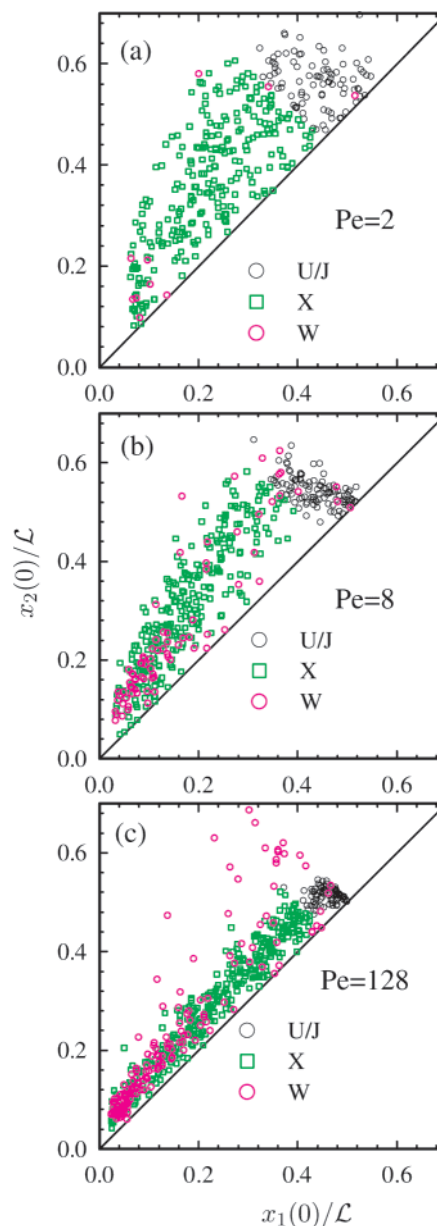


**Figure 7.** Distribution of the long arm  $x_2(0)/L$  vs the short arm  $x_1(0)/L$  for T4-DNA at the onset of unhooking. The solid line is  $x_2(0)/L = x_1(0)/L$ .

the time ( $t$ ) is made nondimensionalized with  $l_p^2/D$  and denoted by  $\hat{t}$ . Overall, the models for the two collision types are consistent with simulation data except for a slight underestimation in the prediction of  $\delta \hat{t}_1$ . It is observed that there is a sharp transition from X to U/J collisions around  $x_1(0)/L \sim 0.4$ . Equation 10 nicely predicts  $\hat{T}_{\text{unhook}}$  of X molecules for  $x_1(0)/L < 0.4$  and eq 6 is consistent with  $\hat{T}_{\text{unhook}}$  of J molecules for  $x_1(0)/L > 0.4$ . Thus,  $x_1(0)/L = 0.4$  can be used as a heuristic criterion to divide the interval into two distinct regions according to dominant collision type (see Supporting Information). It is interesting that a universal crossover point ( $\sim 0.42$ ) between the X and U/J models is predicted by setting eq 6 to equal to eq 10. We can observe that there is a clear linear relationship between  $\hat{T}_{\text{unhook}}$  and  $x_1(0)/L$  in  $x_1(0)/L < 0.4$ , which matches with the X model prediction.

For X molecules (Figure 8, left-hand side), we can observe a clear difference between  $\hat{T}_{\text{H}}$  and  $\hat{T}_{\text{unhook}}$  in functional dependencies on  $x_1(0)/L$ . The model for  $\hat{T}_{\text{unhook}}$  successfully captures the linear relationship between  $\hat{T}_{\text{unhook}}$  and  $x_1(0)/L$  and the model



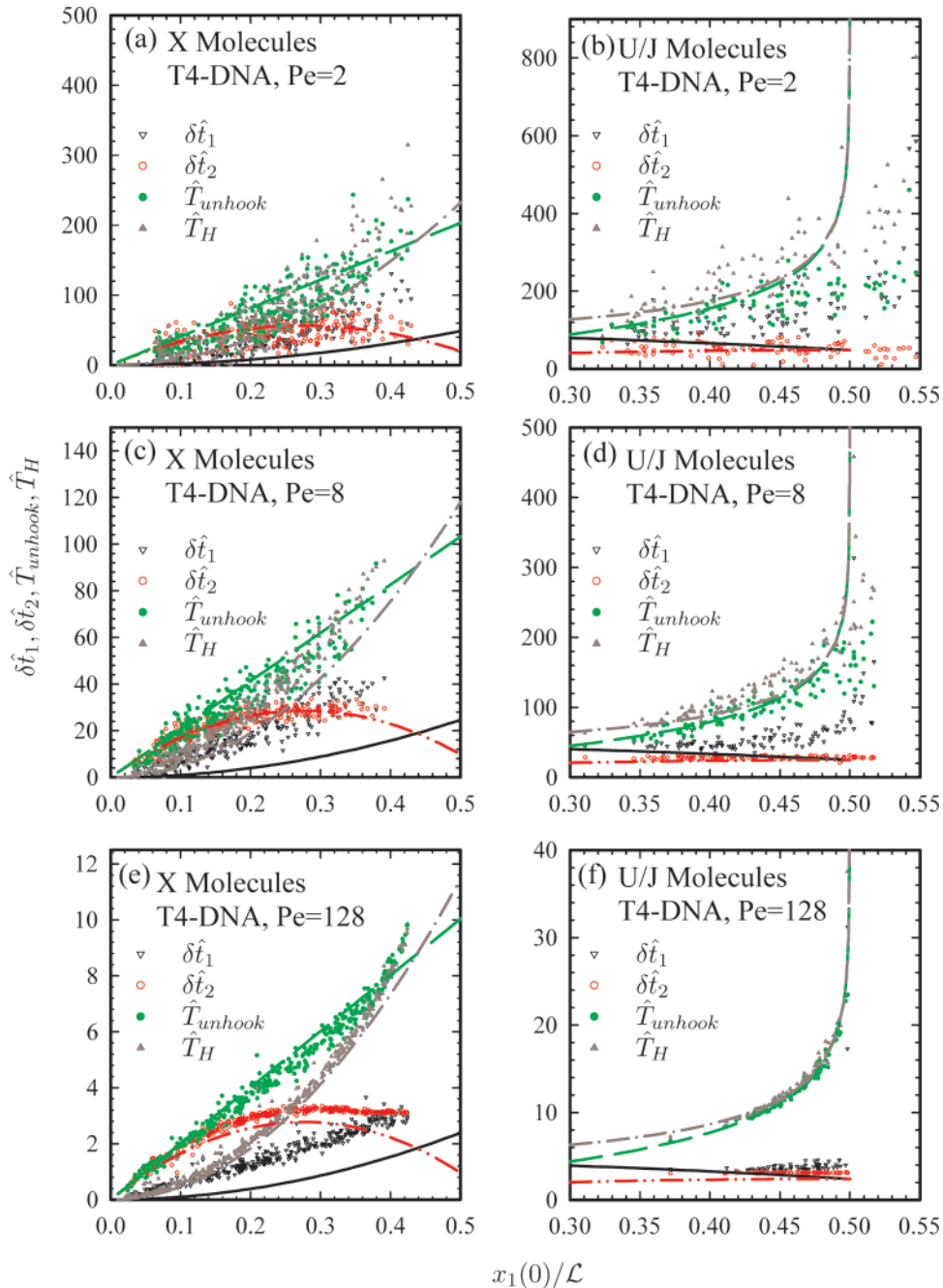


**Figure 8.** Comparison of BD simulation data and models for  $\delta\hat{t}_1$ ,  $\delta\hat{t}_2$ ,  $\hat{T}_H$  and  $\hat{T}_{unhook}$  for X (left-hand side) and U/J (right-hand side) molecules for T4-DNA. In X molecules (left-hand side), black ( $\delta\hat{t}_1$ ), red ( $\delta\hat{t}_2$ ), green ( $\hat{T}_{unhook}$ ) and gray ( $\hat{T}_H$ ) lines correspond to eqs 8, 9, 10 and 11, respectively. In U/J molecules (right-hand side), black ( $\delta\hat{t}_1$ ), red ( $\delta\hat{t}_2$ ), green ( $\hat{T}_{unhook}$ ) and gray ( $\hat{T}_H$ ) lines correspond to eqs 4, 5, 6 and 7, respectively.

for  $\hat{T}_H$  captures the quadratic relationship between  $\hat{T}_H$  and  $x_1(0)/\mathcal{L}$ . Furthermore, both models are in agreement with simulation data on a quantitative level. In the case of U/J molecules (Figure 8, right-hand side), it is observed that  $\hat{T}_{unhook} \rightarrow \hat{T}_H$  as  $x_1(0)/\mathcal{L} \rightarrow 0.5$ . This tendency is more pronounced with increasing  $Pe$  as shown in Figure 8 (right-hand side).

In Figure 9, we present  $\hat{T}_H$  vs  $\hat{T}_{unhook}$  at varying molecular weights (left-hand side) and  $Pe$  numbers (right-hand side). At low  $Pe$  (Figure 9b), it is not clear if the scaling law between  $\hat{T}_H$  and  $\hat{T}_{unhook}$  is different for two collision types. The scattering can be attributed to Brownian motion, which is more important at low  $Pe$ . With increasing  $Pe$ , the figure clearly shows different scaling laws according to eqs 12 and 13. Furthermore, the difference in scaling laws between  $\hat{T}_H$  vs  $\hat{T}_{unhook}$  becomes clearer with increasing molecular weight (Figure 9, left-hand side).

In Figure 10, we present simulation data for  $\hat{T}_H$  vs  $x_1(0)/\mathcal{L}$  and compare the modified X (eq 11), modified J (eq 7), and original U/J (eq 6) models with numerical data. In the figure, eqs 11 and 7 are consistent with the data in the regions  $x_1(0)/\mathcal{L} < 0.4$  and  $x_1(0)/\mathcal{L} > 0.4$ , respectively. Interestingly, eq 6 is consistent with the data over the entire range of  $x_1(0)/\mathcal{L}$ . Equation 7 approaches eq 6 as  $x_1(0)/\mathcal{L} \rightarrow 0.5$ . For  $x_1(0)/\mathcal{L} < 0.4$ , eq 6 is closer to data than eq 11. We surveyed the root-mean-square error (rmse) between eqs 11 and 6 and the numerical data for X molecules with  $x_1/\mathcal{L} < 0.4$ . For all cases explored in this study, the rmse of the original U/J model (eq 6) were smaller than those of the modified X model (eq 11) but the relative difference between two models becomes smaller with increasing molecular weight at high  $Pe$  (see Supporting Information). Thus, it is expected that eq 6 can be used as a heuristic model for  $T_H$  for

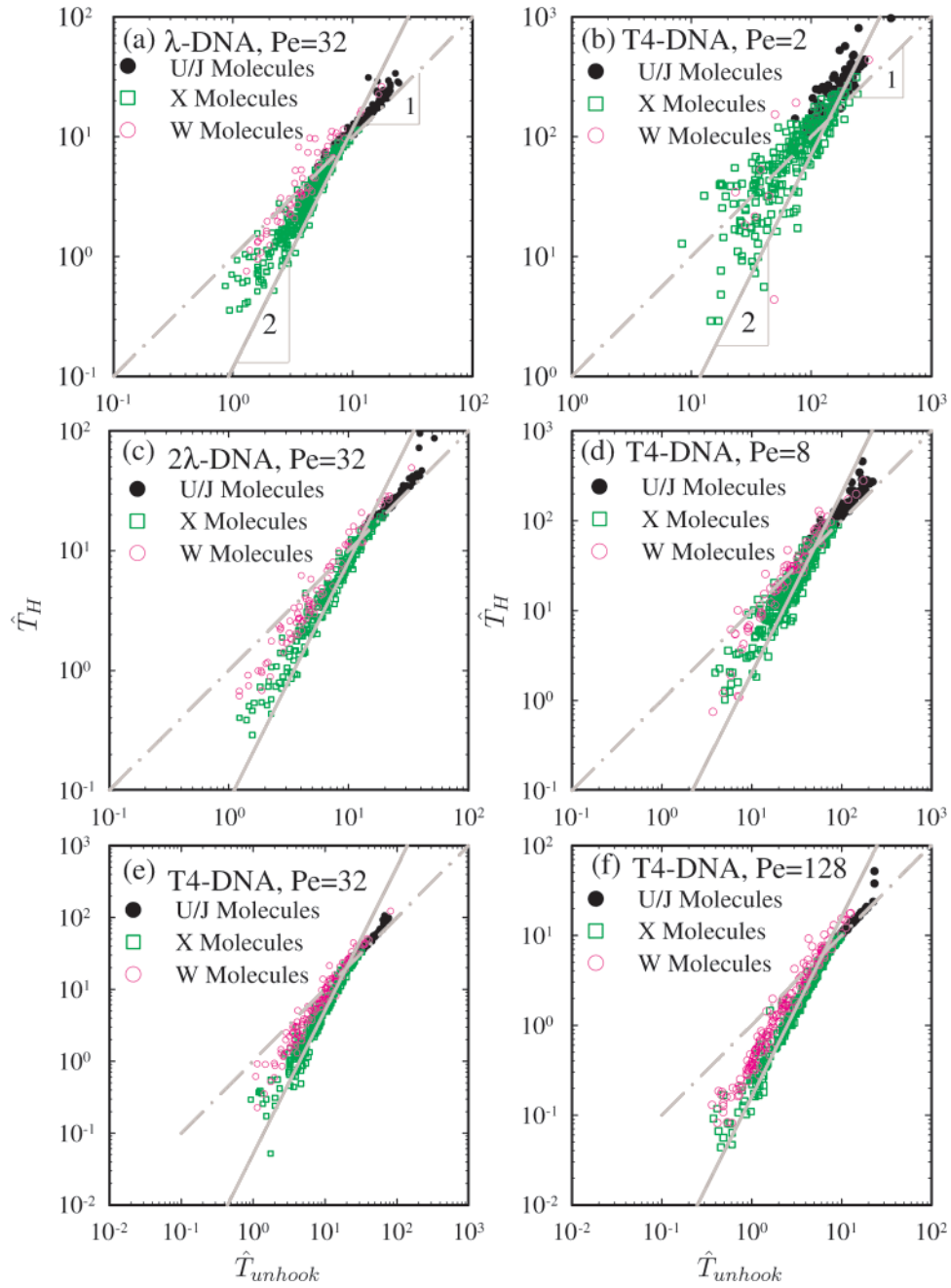


**Figure 9.** Scaling laws between  $\hat{T}_H$  and  $\hat{T}_{unhook}$  at varying molecular weights (left-hand side) and  $Pe$  numbers (right-hand side).

the entire  $x_1(0)/\mathcal{L}$  region. Some W molecules significantly deviate from eq 11 or 6. Nevertheless, the hold-up times of most W molecules are still quite close to the model curves and thus, it is expected that the deviations do not greatly contribute to the mean hold-up time.

**Mean Hold-up Time**

In the previous sections, we verified that the proposed micromechanical models successfully predict simulation data. In this section, we will derive the mean hold-up time (eq 15) based on existing micromechanical models using the observed probability distributions for  $\hat{x}$  (eqs 16 and 17). The generic form of the micromechanical models for hold-up time can be denoted by  $\mathcal{L}/\mu E_0 f(\hat{x})$  (cf. eqs 6, 7, 11, and 14). Thus, we can derive the mean hold-up time  $\langle \hat{T}_H \rangle$  by determining  $\mathcal{L}(Pe)$ ,  $f(\hat{x})$  and the probability distribution of  $\hat{x}$  at a given  $Pe$ .

**Fractional Stretching ( $\mathcal{L}/L$ ).** In this section, we will derive a relationship for fractional stretching ( $\mathcal{L}/L$ ) vs  $Pe$  for a DNA molecule with the central bead tethered at the front cylinder wall ( $\theta = 0$ ). We assume that the cylinder size is negligible, and thus, there is uniform electric field. In the high force limit, Marko and Siggia<sup>28</sup> derived the extension-force relationship for a tethered DNA molecule with one free end in uniform electric field:

$$\mathcal{L}/L \approx 1 - \frac{1}{(Pe)^{1/2}} \text{ as } Pe \rightarrow \infty \tag{18}$$

However, the above equation cannot be applied in the low  $Pe$  limit, i.e., it predicts  $\mathcal{L}/L = 0$  at  $Pe = 1$ . In low  $Pe$  limit,<sup>36</sup> it is predicted that  $\mathcal{L}/L \approx 1/6 Pe$  (cf. the prefactor  $\sim 1/6$  was obtained considering the slowest mode for large  $N_b$  at steady state in eq 10 of ref 36). The next mode only introduces a  $\sim 4\%$

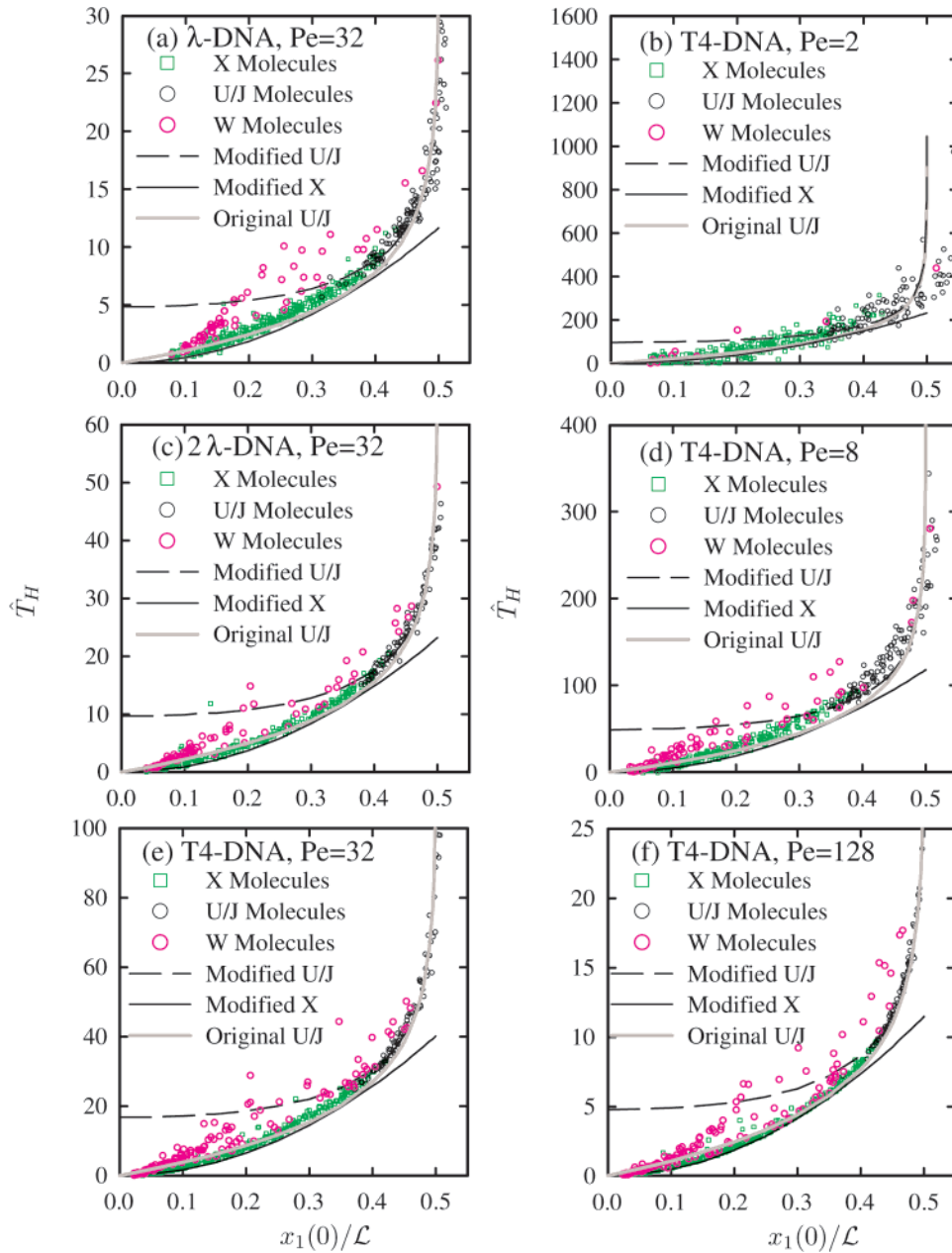


**Figure 10.** Comparison of models and simulation data at varying molecular weights (left-hand side) and  $Pe$  numbers (right-hand side). The lines (modified U/J, modified X and original U/J) correspond to eqs 7, 11 and 6, respectively.

change and so was neglected. Both asymptotic behaviors at low and high  $Pe$  limits are similar to those of the original M–S force law. Thus, the fractional extension– $Pe$  relationship can be expressed as follows:

$$\frac{1}{4} Pe = \frac{\mathcal{L}}{L} + \frac{1}{4(1 - (\mathcal{L}/L))^2} - \frac{1}{4} \quad (19)$$

Therefore, the fractional stretching– $Pe$  relationship can be denoted as follows:

$$\mathcal{L}/L = g^{-1}(Pe) \quad (20)$$

Here  $g^{-1}(Pe)$  is the inverse function of eq 19. We showed that the data lies close to eq 20, which has no adjustable parameters (see Supporting Information).

**Derivation of Mean Hold Time.** Plugging eq 14 into eq 15 (the effect of center-of-mass movement during unraveling

and unhooking is ignored for this model), eq 15 can be expressed as follows:

$$\langle T_H \rangle = \int_0^1 p(\hat{x}_0)(-t_c/2) \ln \hat{x}_0 d\hat{x}_0 \quad (21)$$

After eq 17 is plugged into the above equation, the integration results in the following relationship:

$$\langle T_H \rangle = 1.65 \frac{\mathcal{L}}{\mu E_0} \quad (22)$$

Now, by applying eq 20 to the above equation and nondimensionalizing  $\langle T_H \rangle$  with  $l_p^2/D$ , eq 22 can be expressed as follows:

$$\langle \hat{T}_H \rangle / (L/l_p) = 1.65/Pe \times g^{-1}(Pe) \quad (23)$$

In addition to the conventional rope-over-pulley model, we consider two different micromechanical models to derive mean

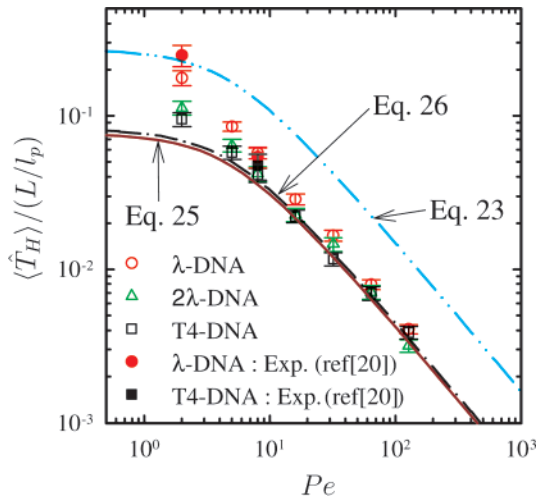


**Figure 11.** Mean hold-up time ( $\langle \hat{T}_H \rangle / (L/l_p)$ ) vs  $Pe$ .

hold-up time using  $x_1(0)/\mathcal{L}$ . First, we use a combination of the modified U/J and the modified X models (eqs 7 and 11 proposed by Randall and Doyle<sup>20</sup>). Next we consider the original U/J model (eq 6) as a heuristic model. Equation 16 will be commonly used for the probability distribution of  $x_1(0)/\mathcal{L}$ .

We apply the modified X (eq 11) and modified U/J models (eq 7) to eq 15 for  $x_1(0)/\mathcal{L} < \alpha$  and  $\alpha < x_1(0)/\mathcal{L} < 0.5$ , respectively.

$$\langle T_H \rangle = \int_0^\alpha p(\hat{x}_1) [4.8t_c \hat{x}_1^2] d\hat{x}_1 + \int_\alpha^{0.5} p(\hat{x}_1) [t_c (-1/2 \ln(1 - 2\hat{x}_1) + 1/2 - \hat{x}_1)] d\hat{x}_1 \quad (24)$$

where  $\hat{x}_1$  denotes  $x_1(0)/\mathcal{L}$ .  $\alpha$  is heuristically chosen as 0.4 for the transition point of  $x_1(0)/\mathcal{L}$  from the X to U/J regime as observed in Figure 10. After plugging eqs 16 and 20 into the above equation, the nondimensionalized mean hold-up time is

$$\langle \hat{T}_H \rangle / (L/l_p) = 0.47/Pe \times g^{-1}(Pe) \quad (25)$$

In eq 24, we computed that the relative contribution of the first and second terms to the mean hold-up time is 43% and 57%, respectively. This means that when a uniform probability distribution for  $x_1(0)/\mathcal{L}$  is assumed, the contribution of U/J molecules to the mean hold-up time is more than half, though they represent only  $\sim 20\%$  of the ensemble.

In the previous section, we observe that the original U/J model (eq 6) can be a good heuristic model to describe  $T_H$  for the whole  $x_1(0)/\mathcal{L}$  region. We plug eq 6 and eq 16 into eq 15, and after applying eq 20, we get the nondimensionalized mean hold-up time for this heuristic model:

$$\langle \hat{T}_H \rangle / (L/l_p) = 0.5/Pe \times g^{-1}(Pe) \quad (26)$$

Note that eq 25 and eq 26 are nearly identical, and eqs 23, 25, and 26 only differ by a constant prefactor.

**Comparison of Derived Mean Hold-up Times with Simulation and Experimental Data.** In Figure 11, we compare the nondimensionalized mean hold-up time ( $\langle \hat{T}_H \rangle / (L/l_p)$ ) to our simulation data, previous experimental data<sup>20</sup> and the derived equations for mean hold-up time (eqs 23, 25 and 26). Overall, our simulation data show good qualitative and quantitative agreement with existing experimental data but there is small deviation at low  $Pe$ . The simulation data collapse for  $Pe \geq 8$  and are consistent with the two derived equations for the mean hold-up time (eqs 25 and 26).

Second, the conventional rope-over-pulley model overestimates the mean hold-up time (eq 23) compared with simulation and experimental data as shown in Figure 11. The rope-over-pulley model (eq 14) predicts a longer hold-up time for shorter  $x_0(0)/\mathcal{L}$ . We assumed that the probability distribution of  $x_0(0)/\mathcal{L}$  is uniform for  $x_0(0)/\mathcal{L} < 0.1$  and is 0 for  $x_0(0)/\mathcal{L} > 0.1$  which is strictly only valid at high  $Pe$ . black As shown in Table 1, the majority of the ensemble is made up of X collisions at high  $Pe$ , and as shown in Figure 7c, most of these X molecules have small  $x_0(0)/\mathcal{L}$ . As previously discussed, the unhooking mechanism of an X collision is totally different from that of a U/J collision, i.e., the unhooking dynamics of an X collision is governed not by  $x_0(0)/\mathcal{L}$  but by  $x_1(0)/\mathcal{L}$ . Thus, the rope-over-pulley model, which is based on constant  $\mathcal{L}$  during unhooking, is limited to a small portion of collisions. Therefore, mean hold-up time predictions based solely on the rope-over-pulley model are inconsistent with simulation and experimental data.

In Figure 11, clear different asymptotic behaviors for ( $\langle \hat{T}_H \rangle / (L/l_p)$ ) are found at low and high  $Pe$  limits, respectively. At low  $Pe$ , eqs 22, 24, and 25 are predicted to be constant since  $g^{-1}(Pe)$  is linearly proportional to  $Pe$  and thus ( $\langle \hat{T}_H \rangle / (L/l_p)$ ) is predicted to be constant in this regime. On the other hand,  $g^{-1}(Pe)$  approaches unity at large  $Pe$ , and thus, eqs 23, 25, and 26 are  $\sim 1/Pe$ .

There is negligible difference between the predictions of eq 25 and 26, both of which are consistent with experimental data, except at low  $Pe$ . The deviation at low  $Pe$  increases with decreasing molecular weight. This can be attributed to the increasing fraction of U/J molecules with decreasing molecular weight as shown in Table 1. In the previous section, we computed the relative contribution from X and U/J molecules in the mean hold-up time. A larger probability distribution of  $x_1(0)/\mathcal{L}$  near 0.5 as shown in Figure 5a will result in a larger mean hold-up time than predicted by models based on assuming a uniform probability distribution.

The derived equations can be applied to a practical  $Pe$  region ( $Pe \geq O(10)$ ), which is typical of experimental conditions.<sup>5</sup> Thus, it is expected that the derived mean hold-up time can be helpful in designing post arrays and also give physical insight of this problem.

## Conclusion

BD simulation was employed to investigate the dynamics of DNA collisions with a cylindrical obstacle. The present work expands upon the findings of previous experimental and modeling studies.<sup>20</sup> Simulation has enabled us to probe a much wider parameter space than in the previous experiments<sup>20</sup> and more conclusively validate various aspects of the micromechanical models proposed by Randall and Doyle.<sup>20</sup> Our results lend strong support to the notion that X collisions are indeed the most dominant collision type. Surprisingly, this mode of collision was overlooked in previous simulations. Our new contribution to the models is to derive an analytical expression for mean fractional extension as a function of  $Pe$  that makes the micromechanical models of Randall and Doyle fully predictive. In addition, the stochastic nature of the process is embodied in our postulated simple forms for the probability distribution of the initial arm lengths. Taken together, these expressions provide a simple expression for the mean hold-up time which is fairly accurate at large  $Pe$ . We expect that our present work can shed light on the understanding of general polyelectrolyte collisions with an obstacle. The simulation method can be easily extended to study post arrays. It is also anticipated that the derived mean hold-up time can be combined



with mesoscale transport theories (e.g., using a continuous time random walk framework<sup>7,19</sup>) to more accurately model DNA separations in post arrays.

**Acknowledgment.** This work was supported by NSF NIRT Grant No. CTS-0304128. We thank Aruna Mohan for her insightful comments.

**Supporting Information Available:** A figure showing representative center-of-mass trajectories, tables to show the sensitivity to  $\delta_{cr}$  and the effect of the modeling factors to reproduce  $\bar{X}$  collisions, and figures showing comparison of models and  $\hat{T}_{unhook}$  from simulations, relative difference between rmse of eq 11 and that of eq 6, and  $\mathcal{L}/L$  vs  $Pe$ . This material is available free of charge via the Internet at <http://pubs.acs.org>.

## References and Notes

- (1) Viovy, J.-L. *Rev. Mod. Phys.* **2000**, *72*, 813.
- (2) Volkmuth, W. D.; Austin, R. H. *Nature (London)* **1992**, *358*, 600.
- (3) Doyle, P. S.; Bibette, J.; Bancaud, A.; Viovy, J.-L. *Science* **2002**, *295*, 2237.
- (4) Kaji, N.; Tezuka, Y.; Takamura, Y.; Ueda, M.; Nishimoto, T.; Nakanishi, H.; Horiike, Y.; Baba, Y. *Anal. Chem.* **2004**, *76*, 15.
- (5) Minc, N.; Fütterer, C.; Dorfman, K. D.; Bancaud, A.; Gosse, C.; Goubault, C.; Viovy, J.-L. *Anal. Chem.* **2004**, *76*, 15.
- (6) Minc, N.; Bokov, P.; Zeldovich, K. B.; Fütterer, C.; Viovy, J.-L.; Dorfman, K. D. *Electrophoresis* **2005**, *26*, 362.
- (7) Minc, N.; Viovy, J.-L.; Dorfman, K. D. *Phys. Rev. Lett.* **2005**, *94*, 198105.
- (8) Chan, E. Y.; Goncalves, N. M.; Haeusler, R. A.; Hatch, A. J.; Larson, J. W.; Maletta, A. M.; Yantz, G. R.; Carstea, E. D.; Fuchs, M.; Wong, G. G.; Gullans, S. R.; Gilmanshin, R. *Genome Res.* **2004**, *14*, 1137.
- (9) Song, L.; Maestre, M. F. *J. Biomol. Struct. Dyn.* **1991**, *9*, 087.
- (10) Sevick, E. M.; Williams, D. R. M. *Phys. Rev. E* **1994**, *50*, R3357.
- (11) André; Long, D.; Ajdari, A. *Eur. Phys. J. B* **1998**, *4*, 307.
- (12) Saville, P. M.; Sevick, E. M. *Macromolecules* **1999**, *32*, 892.
- (13) Sevick, E. M.; Williams, D. R. M. *Europhys. Lett.* **2001**, *56*, 529.
- (14) Patel, P. D.; Shaqfeh, E. S. G. *J. Chem. Phys.* **2003**, *118*, 2941.
- (15) Kenward, M.; Slater, G. W. *Eur. Phys. J. E* **2006**, *20*, 125.
- (16) Volkmuth, W. D.; Duke, T.; Wu, M. C.; Austin, R. H. *Phys. Rev. Lett.* **1994**, *28*, 2117.
- (17) Brochard-Wyart, F.; Hervet, H.; Pincus, P. *Europhys. Lett.* **1994**, *26*, 511.
- (18) Brochard-Wyart, F. *Europhys. Lett.* **1995**, *30*, 387.
- (19) Dorfman, K. D. *Phys. Rev. E* **2006**, *73*, 061922.
- (20) Randall, G. C.; Doyle, P. S. *Macromolecules* **2006**, *39*, 7734.
- (21) Randall, G. C.; Doyle, P. S. *Phys. Rev. Lett.* **2004**, *93*, 1137.
- (22) Randall, G. C.; Doyle, P. S. *Macromolecules* **2005**, *38*, 2410.
- (23) Chen, Y.-L.; Graham, M. D.; de Pablo, J. J.; Randall, G. C.; Gupta, M.; Doyle, P. S. *Phys. Rev. E* **2004**, *70*, 060901.
- (24) Tlusty, T. *Macromolecules* **2006**, *39*, 3927.
- (25) Balducci, A.; Mao, P.; Han, J.; Doyle, P. S. *Macromolecules* **2006**, *39*, 6274.
- (26) Heyes, D.; Melrose, J. J. *Non-Newtonian Fluid Mech.* **1993**, *46*, 1.
- (27) Kim, J. M.; Doyle, P. S. *J. Chem. Phys.* **2006**, *125*, 074906.
- (28) Marko, J. F.; Siggia, E. D. *Macromolecules* **1995**, *28*, 8759.
- (29) Underhill, P. T.; Doyle, P. S. *J. Non-Newton. Fluid Mech.* **2004**, *122*, 3.
- (30) Bustamante, C.; Marko, J. F.; Siggia, E. D.; Smith, S. *Science* **1994**, *265*, 1599.
- (31) Jendrejack, R. M.; Graham, M. D.; de Pablo, J. J. *J. Chem. Phys.* **2002**, *116*, 7752.
- (32) Jendrejack, R. M.; Schwartz, D. C.; Graham, M. D.; de Pablo, J. J. *J. Chem. Phys.* **2003**, *119*, 1165.
- (33) Jendrejack, R. M.; Schwartz, D. C.; Graham, M. D.; de Pablo, J. J. *J. Chem. Phys.* **2004**, *120*, 2513.
- (34) Li, L.; Madras, N.; Sokal, A. J. *Stat. Phys.* **1995**, *80*, 661.
- (35) Nixon, G. I.; Slater, G. W. *Phys. Rev. E* **1994**, *50*, 5033.
- (36) Mohan, A.; Doyle, P. S. *Macromolecules* **2007**, *40*, 4301.
- (37) Warner, H. R. *Ind. Eng. Chem. Fundam.* **1972**, *11*, 379.

MA0710434